Structural Engineering and Mechanics, Vol. 41, No. 6 (2012) 805-822
DOI: http://dx.doi.org/10.12989/sem.2012.41.6.805

Buckling response of offshore pipelines under combined tension and bending

Shun-feng Gong*, Xing-yue Ni, Lin Yuan and Wei-liang Jin

Institute of Structural Engineering, Zhejiang University, Hangzhou, 310058, China

(Received October 17, 2009, Revised February 22, 2012, Accepted February 23, 2012)

Abstract. Offshore pipelines have to withstand combined actions of tension and bending during deepwater installation, which can possibly lead to elliptical buckle and even catastrophic failure of whole pipeline. A 2D theoretical model initially proposed by Kyriakides and his co-workers which carried out buckling response analysis of elastic-plastic tubes under various load combinations, is further applied to investigate buckling behavior of offshore pipelines under combined tension and bending. In association with practical pipe-laying circumstances, two different types of loadings, i.e., bent over a rigid surface in the presence of tension, and bent freely in the presence of tension, are taken into account in present study. In order to verify the accuracy of the theoretical model, numerical simulations are implemented using a 3D finite element model within the framework of ABAQUS. Excellent agreement between the results validates the effectiveness of this theoretical method. Then, this theoretical model is used to study the effects of some important factors such as load type, loading path, geometric parameters and material properties etc. on buckling behavior of the pipes. Based upon parametric studies, a few significant conclusions are drawn, which offer a theoretical reference for design and installation monitoring of deepwater pipelines.

Keywords: offshore pipeline; deepwater; buckling; pipe-laying

1. Introduction

Offshore pipeline plays an important role in oil and gas exploitation projects. The installation of pipelines, especially in deep water, can induce rather severe loads to the structure. The Pipes have to withstand combined actions of tension and bending regardless of the installation method used (S-lay, J-lay or reeling-lay) (Kashani and Young 2005, Li *et al*. 2008). Two types of loadings can be categorized according to whether there exist any transverse loading at the surface. Type A simulates the buckling behavior of the pipes bent over a rigid and curved surface with simultaneous tension applied. This kind of loading case is mainly experienced when a pipe goes over a stinger in deepwater S-lay operation or winds onto a large diameter reel in reeling installation. Type B is concerned with loading conditions of the pipes in suspended section which are bent freely in the presence of axial tension. Under such combined loads, the pipelines are vulnerable to local buckling, which will have a potential of resulting in failure of whole structure as well as huge economic loss.

*Corresponding author, Associate Professor, E-mail: sfgong@zju.edu.cn

The buckling response of the pipes under different load combinations has drawn much attention in the past few decades. Gellin (1980) investigated the effect of nonlinear material behavior on the buckling of an infinitely long cylindrical shell under pure bending. Subsequently, the response and stability of elastic-plastic circular tubes under combined bending and external pressure were analyzed by Kyriakides and Shaw (1982). They determined the maximum moment and curvature as a function of material and geometric parameters for different pressures. Besides, inelastic analyses for circular tubes under cyclic bending were carried out later (Shaw and Kyriakides 1985). Dyau and Kyriakides (1992) developed a 2D theoretical model to examine buckling response of the tubes under combined bending and tension. Al-Sharif and Preston (1996) proposed a deterministic model to calculate the collapse under combined bending and pressure, and developed a numerical model to simulate the plastic collapse of thick-walled pipe. Moreover, it was found that the simulation results agreed well with those of the deterministic model. Xue and Fatt (2002) developed the analytical solutions for elastic buckling of a non-uniform, long cylindrical shell under external pressure, the buckling modes of the pipe cross-section were found to be dependent on relative thickness of two different regions and angular extent of the section with reduced thickness. Studies on the collapse of thick-walled tubes under three different load combinations, i.e., bending and pressure, tension and pressure, and tension and bending, were performed respectively by Kyriakides and Corona (2007). Later, Yuan *et al*. (2009) investigated buckling response of offshore pipelines subjected to pure bending, combined bending and external pressure. It is indicated that the buckling of the pipe is closely related to diameter-to-thickness ratio (D/t), and the existence of initial curvature will weaken the load-carrying capacity of the pipe to resist external hydrostatic pressure. In addition, Gong *et al.* (2011) firstly conducted the analysis of buckling response of offshore pipelines under simultaneous tension, bending, and external pressure, and pointed out that loading paths and axial tension have a remarkable effect on buckling behaviors of the tubes.

It is noted that the aforementioned research efforts focus on the local buckling of the tubes under various load combinations. However, these load combinations scarcely linked with actual force states of offshore pipeline in deepwater pipe-laying process. Accordingly, the buckling response of offshore pipelines in association with practical pipe-laying circumstances still deserves further study. A 2D theoretical model initially proposed by Kyriakides and his co-workers are further applied to conduct buckling response analysis of offshore pipelines under combined tension and bending, two different types of loadings, i.e., bent over a rigid surface in the presence of tension, and bent freely in the presence of tension, are taken into account in present study. Meanwhile, a 3D finite element model is developed under the same loading conditions using ABAQUS, and the comparison of the results between the two methods is carried out. It is found that the results match well with each other, which verifies the accuracy of this theoretical model. Furthermore, the buckling response is studied in detail corresponding to the loading path $T \rightarrow \kappa$ (Type A), in which the pipe is first tensioned to a chosen value T, and then the curvature κ is applied. This loading path considered can more approximate the case of the pipeline over a stinger in deepwater S-lay process. Besides, a parametric study concerning some important influencing factors is conducted, which offers a theoretical reference for design and installation monitoring of deepwater pipelines.

2. Theoretical formulations

Kyriakides and his co-worker (Kyriakides and Shaw 1982, Shaw and Kyriakides 1985, Ju and

Kyriakides 1991, Kyriakides and Corona 2007) systematically presented a 2D nonlinear ring theoretical model for buckling and collapse of the tubes. In this theoretical model, the tube surface was modeled as thin shell, using the formulation proposed by Sanders (1963) for small strains and large displacements. The material behavior was described by the J_2 flow theory of plasticity with isotropic strain hardening. Based on the virtual work principle, the equilibrium equation of the system in an incremental form was obtained, and then the Newton-Raphson method was used to iteratively solve these equations.

2.1 Kinematics

The tube considered in this paper is a long, circular, thick-walled tube, with its mean radius R and wall thickness t. Uniform tension T and curvature κ are assumed to be applied along the length of the tube. As shown in Fig. 1, the displacements of a point on the mid-surface are denoted as u, v and w with respect to axial, circumferential and radial coordinates x, θ and z, respectively.

The kinematic relations must be suitable for ovalization of the tube cross-section. Such a set of relations was originated from thin shell theory presented by Sanders (1963), and then was developed by Gellin (1980) to conduct buckling response analysis of long cylindrical shells under pure bending, and was successfully used by Kyriakides and Shaw (1982) to stability investigations of elastic-plastic circular tubes under combined bending and external pressure. It is assumed that the plane sections normal to the mid-surface of the tube and those normal to the tube wall mid-surface remain plane before and during deformation. Besides, small strain and finite rotations about the axes are assumed herein.

Kyriakides and Shaw (1982) described in detail the following kinematic relations between stains and displacements. The axial strain can be denoted as

$$\varepsilon_x = \varepsilon_x^0 + \varsigma\kappa \tag{1}$$

where ε_x^0 is the axial strain of the neutral axis, ς is the distance from a point in the tube wall to the neutral axis, and may be obtained from Fig. 1 as follows

$$\varsigma = (R+w)\cos\theta - v\sin\theta + z\cos\theta \tag{2}$$

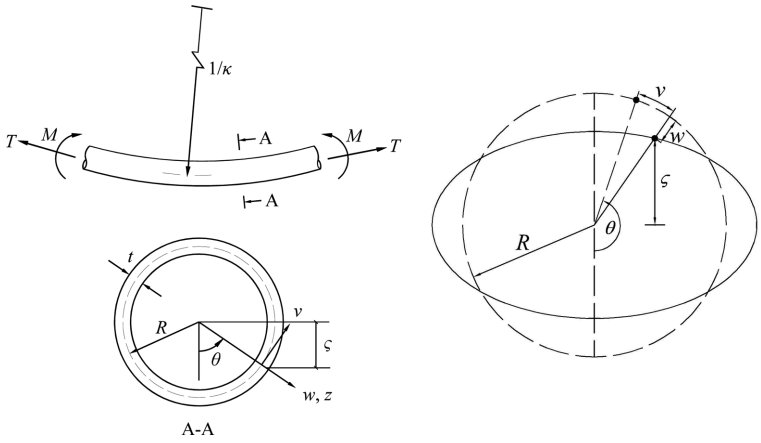

Fig. 1 Geometric parameters and coordinate system

The circumferential strain can be expressed as

$$\varepsilon_\theta = \varepsilon_\theta^0 + z \cdot \kappa_\theta \tag{3}$$

where

$$\varepsilon_\theta^0 = \left(\frac{v' + w}{R}\right) + \frac{1}{2}\left(\frac{v' + w}{R}\right)^2 + \frac{1}{2}\left(\frac{v - w'}{R}\right)^2 \tag{4}$$

and

$$\kappa_\theta = \left(\frac{v' - w''}{R^2}\right) \Big/ \sqrt{1 - \left(\frac{v - w'}{R}\right)^2} \tag{5}$$

where ( )' denotes the differential with respect to θ.

2.2 Constitutive model

The steel material of offshore pipelines exhibits good plastic deformation capacity, and the pipe can be modeled as an elastic-plastic solid. The Ramberg-Osgood model is used to characterize nonlinear stress-strain relationships of the material shown in Fig. 2, which is given as follows

$$\varepsilon = \frac{\sigma}{E}\left[1 + \frac{3}{7}\left|\frac{\sigma}{\sigma_y}\right|^{n-1}\right] \tag{6}$$

where E is Young's modulus, σ_y is the effective yield stress, and n is the material hardening parameter.

The incremental J_2 plastic flow theory with isotropic strain hardening is used to model plastic behavior of the material. The radial stress σ_r and shear stress $\{\sigma_{x\theta}, \sigma_{\theta r}, \sigma_{rx}\}$ are disregarded due to the fact that these components are quite small when comparing with those in the axial and circumferential directions. Therefore, the incremental constitutive model proposed by Kyriakides and Conora (2007) can be further simplified as

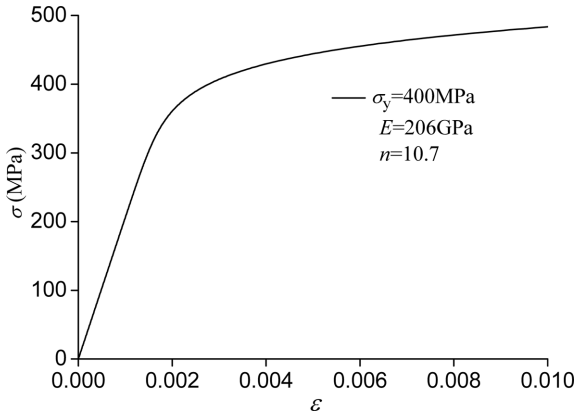

Fig. 2 Stress-strain curve for the Ramberg-Osgood model

$$\begin{Bmatrix} \dot{\varepsilon}_x \\ \dot{\varepsilon}_\theta \end{Bmatrix} = \frac{1}{E}\begin{bmatrix} 1+Q(2\sigma_x-\sigma_\theta)^2 & -\upsilon+Q(2\sigma_x-\sigma_\theta)(2\sigma_\theta-\sigma_x) \\ -\upsilon+Q(2\sigma_x-\sigma_\theta)(2\sigma_\theta-\sigma_x) & 1+Q(2\sigma_\theta-\sigma_x)^2 \end{bmatrix}\begin{Bmatrix} \dot{\sigma}_x \\ \dot{\sigma}_\theta \end{Bmatrix} \tag{7}$$

$$Q = \begin{cases} 0, & \sigma_e \le \sigma_{e\max} \\ \dfrac{1}{4\sigma_e^2}\left(\dfrac{E}{E_t}-1\right), & \sigma_e > \sigma_{e\max} \end{cases} \tag{8}$$

where $(\bullet)$ denotes an increment in $(\,)$, σ_e is the equivalent stress, and $E_t = E_t(\sigma_e)$ is the tangent modulus of the material. They are given as follows

$$\sigma_e^2 = \frac{3}{2}S_{ij}S_{ij} \tag{9}$$

$$\frac{1}{E_t} = \frac{1}{E}\left[1+\frac{3}{7}n\left(\frac{\sigma_e}{\sigma_y}\right)^{n-1}\right] \tag{10}$$

where

$$S_{ij} = \sigma_{ij} - \frac{1}{3}\sigma_{kk}\delta_{ij} \tag{11}$$

where S_{ij} is the deviatoric stress tensor, σ_{ij} is the stress tensor, σ_{kk} is the first invariant of stress tensor, and δ_{ij} is the Kronecker Delta function.

2.3 Principle of virtual work

According to the principle of virtual work, the following equilibrium equation in an incremental form may be obtained

$$2R\int_0^{\pi}\int_{-t/2}^{t/2}(\hat{\sigma}_x\delta\dot{\varepsilon}_x+\hat{\sigma}_\theta\delta\dot{\varepsilon}_\theta)dzd\theta = \delta\dot{W} \tag{12}$$

where $(\hat{\bullet}) \equiv (\bullet + \dot{\bullet})$, and δW is the virtual work of external loads.

It is assumed that the deformation of the cross section, i.e., the in-plane displacements w and v, are symmetric about the axis $\theta = 0$, and they are the functions of θ. Therefore, w and v can be approximated by the following series expansions (Gellin 1980)

$$w \cong R\sum_{n=0}^{N} a_n \cos n\theta, \qquad v \cong R\sum_{n=1}^{N} b_n \sin n\theta \tag{13}$$

Load type A. Bent over a rigid surface in the presence of tension

The tube is assumed to be in contact with the rigid surface with definite curvature κ all the time, and deform uniformly along the longitudinal direction. When tension is increased, the rigid surface is assumed to expand uniformly such that it always remains in contact with the tube, as show in Fig. 3. This boundary condition for zero displacement constraint can be introduced through a Lagrange multiplier. Therefore, the virtual work increment of the external loads can be given by

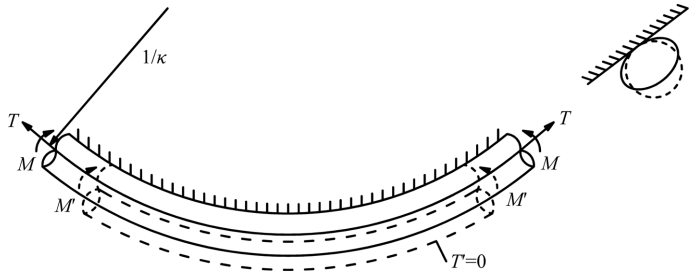

Fig. 3 Bent over a rigid surface in the presence of tension (Type A)

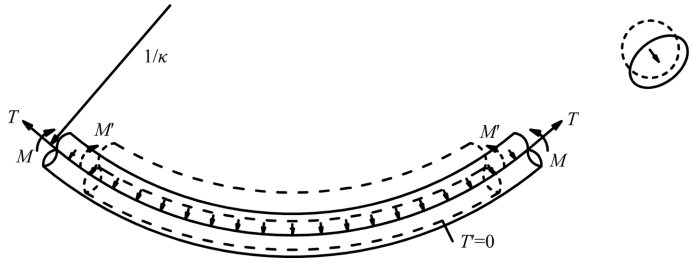

Fig. 4 Bent freely in the presence of tension (Type B)

$$\delta\dot{W} = \hat{T}\delta\dot{\varepsilon}_x^0 - \lambda\delta\dot{w}(\pi) \tag{14}$$

where λ is a Lagrange multiplier, $\delta\dot{w}(\pi)$ is the displacement of the tube cross section at $\theta = \pi$, and thus the following equation may be derived from Eq. (13)

$$\lambda\delta\dot{w}(\pi) = \lambda[\delta\dot{a}_0 - \delta\dot{a}_1 + \delta\dot{a}_2 - \delta\dot{a}_3 + \ldots(-1)^n\delta\dot{a}_n] \tag{15}$$

Substitute Eqs. (13)-(14) into Eq. (12), a system of $2N+3$ nonlinear algebraic equations can be obtained in terms of $\{\dot{a}_0, \dot{a}_1, \ldots, \dot{a}_N, \dot{b}_1, \dot{b}_2, \dot{b}_3, \ldots, \dot{b}_N, \dot{\varepsilon}_x^0, \lambda\}$.

Type B. Bent freely in the presence of tension

In this case, the tube is bent freely, and the deformation is assumed to be uniform along the length of the tube under combined tension and bending, as shown in Fig. 4. The virtual work of the external loads can be given by

$$\delta\dot{W} = \hat{T}\delta\dot{\varepsilon}_x^0 \tag{16}$$

The series expansions used to approximate w and v should preclude rigid body motion in the circumferential direction and represent four-way symmetry, which are given by

$$w \cong R\sum_{n=0}^{N} a_n \cos n\theta, \qquad v \cong R\sum_{n=2}^{N} b_n \sin n\theta \tag{17}$$

Substitute Eqs. (16)-(17) into Eq. (12), a system of $2N+1$ nonlinear algebraic equations can be obtained in terms of $\{\dot{a}_0, \dot{a}_1, \ldots, \dot{a}_N, \dot{b}_2, \dot{b}_3, \ldots, \dot{b}_N, \dot{\varepsilon}_x^0\}$.

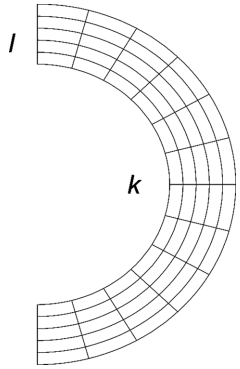

Fig. 5 Distribution of Gaussian integral points

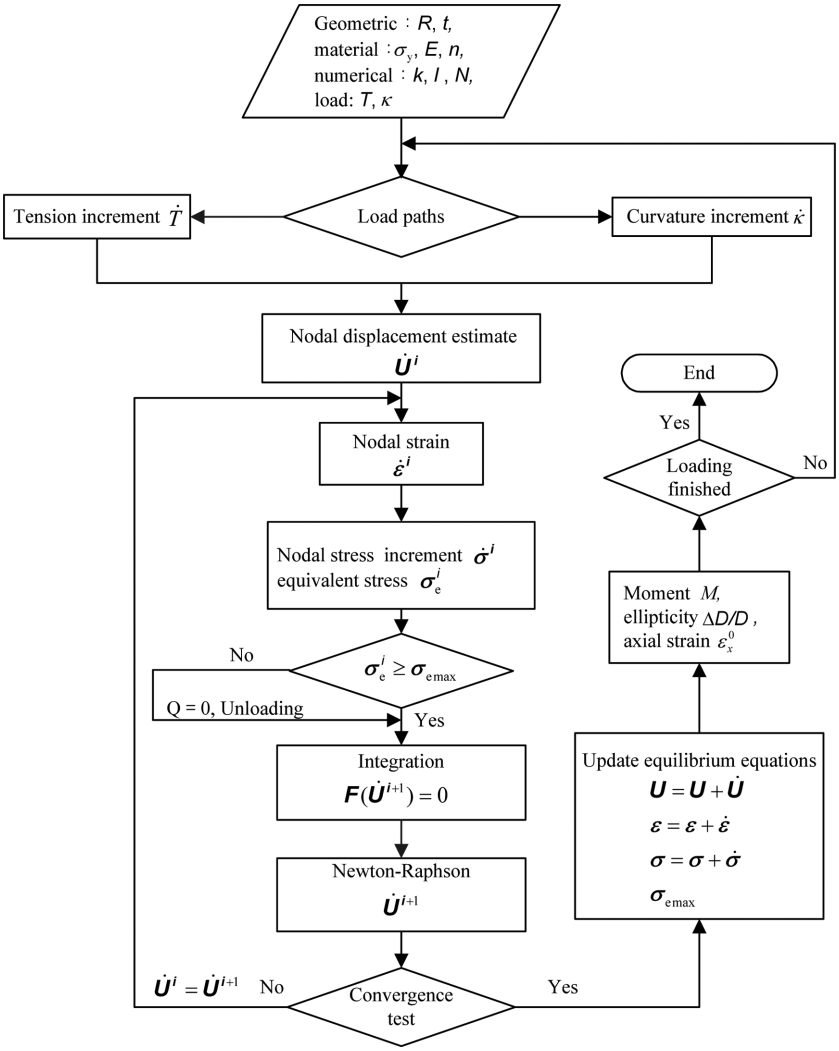

Fig. 6 Flow chart of numerical solution procedure

2.4 Solution method

The resultant $2N + 1$ or $2N + 3$ nonlinear algebraic equations are solved iteratively in the present pipe buckling. Some parameters should be prescribed in advance, namely geometric dimensions, material properties and load types. The number of Gaussian integral points, for the half cross section of the tube, along the circumferential direction and through the thickness is k and l, respectively (Fig. 5).

The main steps of solution procedure for combined loading case are shown in the flow chart in Fig. 6. The tube can be loaded by axial tension T and curvature κ. The loading process is controlled by prescribing the increment of two loading parameters $\{\Delta\kappa, \Delta T\}$. When κ is specified to zero, the case would be that of axial tension. If the prescribed T in the flow chart equals zero, it would reduce to the pure bending case.

The converged solution of previous step is regarded as initial estimate of nodal displacements for the next step. Subsequently, the strain increment can be obtained through the increments of nodal displacements and curvature, and then the stress increment can be achieved. Note that this procedure also involves nested iterations of the constitutive relationship. After obtaining stress components of each integral point, the problem can be solved using the Newton-Raphson method. Strains, stresses as well as displacements corresponding to every integral point are updated when the converged solution is achieved.

After each converged solution, the moment can be obtained

$$M = 2R\int_0^{\pi}\int_{-t/2}^{t/2}\sigma_x\varsigma dz d\theta \tag{18}$$

It is found that the solution can meet the precision requirements when N equals 4 to 6. In the case of pure bending, k = 12 and l = 5 is sufficient. While for the combined case, the mesh should be finer, therefore, k = 12 and l = 7, is found to be adequate.

3. Numerical simulations

A finite element model is developed within the framework of the software ABAQUS to simulate buckling behavior of a pipe under combined tension and bending. 3D, eight-node incompatible solid element, C3D8I, is chosen to model the pipe solid. Since this type of element is enhanced by incompatible modes to bending behavior, it is best suited for present problem (Simo and Armero 1992, Hibbitt *et al*. 2006). The J_2 flow theory of plasticity with isotropic strain hardening is adopted to describe the plastic behavior of the material, and the Ramberg-Osgood constitutive model is used by multi-linear approximations of the stress-strain curve shown in Fig. 2.

The symmetry of the loads and deformations reduces the problem to a quarter of a pipe. As a result, symmetrical boundary conditions are applied at the mid-span (X = 0) and Z = 0 planes (Fig. 7). Besides, additional spring constraints along vertical direction (Y) are applied at the mid-span plane to constrain the rigid body motion. This kind of elastic constraints is desirable for this problem since it can alleviate the stress concentration phenomenon in a certain extent which is inevitable if rigid constraints are applied.

*KINEMATIC COUPLING relationship is imposed between the nodes on the right end of the tube and a reference point (the central node or the bottom one are both suitable). The right end

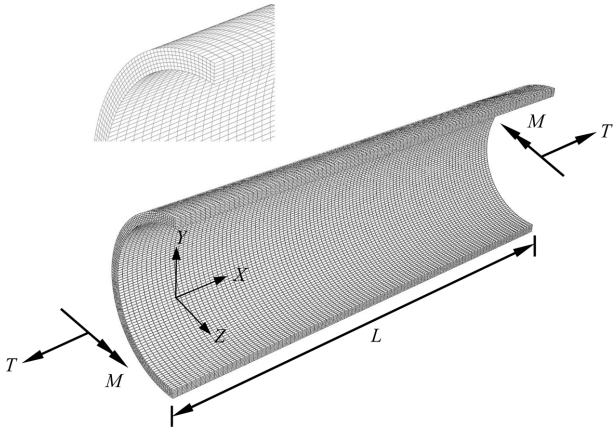

Fig. 7 Finite element mesh and loadings

plane is constrained to remain plane in the loading process, and at the same time the cross section should be free to deform. The curvature is applied by prescribing the angle φ of rotation at the reference point. Likewise, uniform tension is applied to the model through this reference point.

The average curvature of the section can be given by

$$\kappa = \varphi / L \tag{19}$$

To facilitate the development of buckling deformation, the length of the pipe, $L = 3D$ is adopted. The pipe model is meshed into 6 parts through the thickness, 100 parts around the half circumference and 100 parts along the length, which is found to be adequate through trial analysis. Fig. 7 illustrates a typical finite-element mesh used in the analyses. Furthermore, the Nlgeom option is selected for the nonlinear calculation, and the Riks algorithm (arc length method) is adopted here (Hibbitt *et al*. 2006).

4. Results and discussion

4.1 Comparisons of numerical and theoretical results

Numerical simulations and theoretical calculations are carried out respectively for the scenario of *Radial* (κ, T) loading path in load type B. In other words, two loading parameters $\{\Delta\kappa, \Delta T\}$ are simultaneously applied to the model. The analyses are performed for the pipe model based on the parameters of $D = 254$ mm, $D/t = 20$, $E = 206$ GPa, $\sigma_y = 400$ MPa, $n = 10.7$, $\upsilon = 0.3$, $T = 2\ 100$ kN, and $\kappa = 0.16$. The sequence of deformed configuration and stress distribution in the loading process are depicted in Fig. 8.

Included in Fig. 9 is the comparison of the responses calculated by the two methods. As can be seen in the figures, the predicted ellipticity ($\Delta D/D$) of two models is quite close in the overall range. The main reason for the difference is that ABAQUS uses a finite deformation theory whereas the theoretical model is based on small deformation. The other reason for the difference is that the Eq. (19) which is used to calculate the average curvature will generate some discrepancy at high values of loadings. It is observed from Fig. 8 that the phenomenon of stress concentration and local

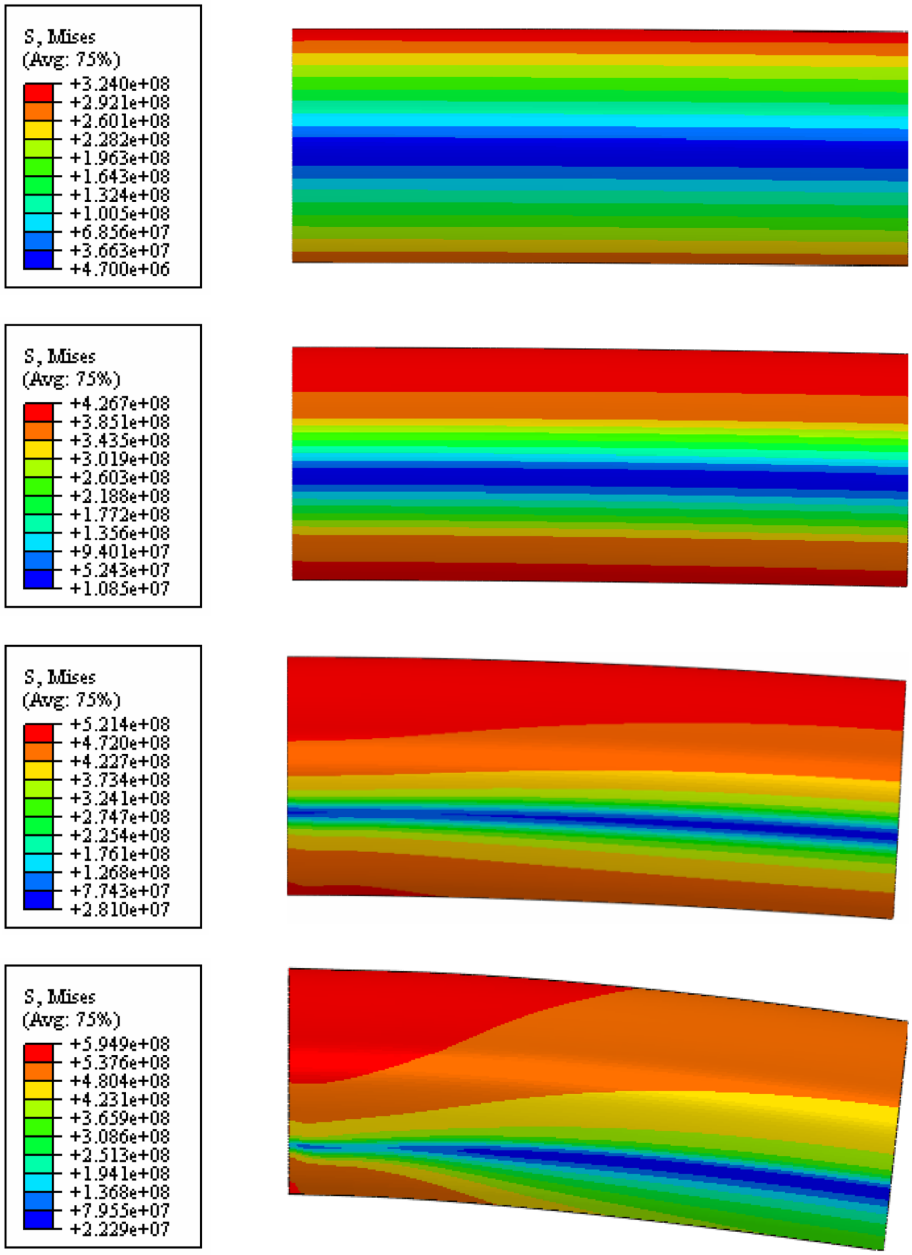

Fig. 8 Deformed configuration and stress distribution in the loading process (Type B)

deformation will become more evident in the region close to the boundary of spring constraints at the mid-span plane when the loads are relatively large, which makes the average curvature obtained becomes somewhat higher compared with the practical condition. It is noted that although these contribute to small differences of ellipticity observed in the figures, the suitability of theoretical method used in predicting buckling response of offshore pipelines has been well verified.

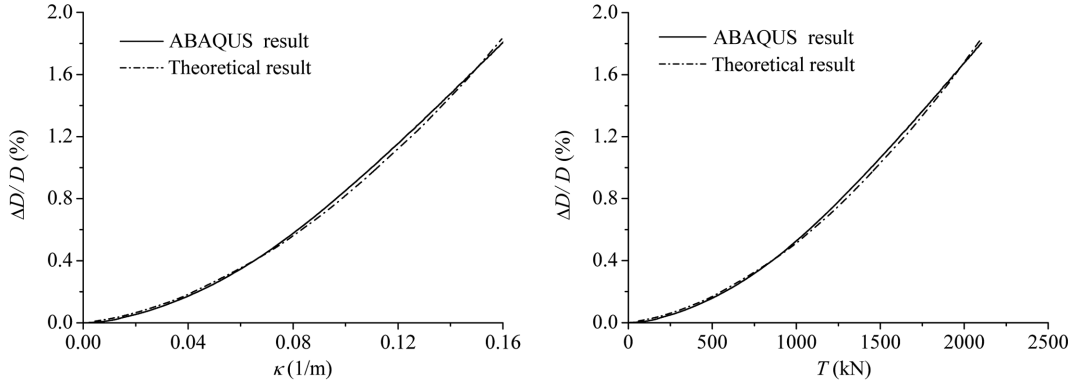

(a) Ellipticity-curvature (b) Ellipticity-tension

Fig. 9 Comparison between the results of theoretical method and numerical simulation

4.2 Illustrative example using theoretical formulations

In this section, the responses of the tubes subjected to two types of loadings, i.e., load type A and load type B, are calculated using the theoretical method. In addition, the comparisons corresponding to three different loading paths are conducted, which are identified as $\kappa \rightarrow T$, $T \rightarrow \kappa$ and *Radial* (κ, T) path, respectively.

Illustrated in Fig. 10 are the buckling responses of the tube under load type A. The analyses are made under the following parameters: D = 304.8 mm, t = 15.24 mm, D/t = 20, E = 206 GPa, σ_y = 400 MPa, n = 10.7 and υ = 0.3. The tube is first bent incrementally to a chosen value κ = 0.2, and then axial load is increased until the values of T = 4 000 kN is reached. Shown in the figures are the predicted moment-curvature, moment-tension, ellipticity-curvature, ellipticity-tension, and axial strain-tension curves.

As can be seen from the figures, in the bending phase of loading history, the growth of bending moment experiences three stages, namely linear increase, nonlinear increase and subsequent plastic plateau. In the following tension-applied phase, redistribution of the stresses leads to a nearly linear drop of the bending moment. In addition, it can be found that the ellipticity is approximately proportional to the curvature at the beginning. However, the nonlinearity becomes more and more notable as the curvature grows. In the phase of tension, its growth is almost linear to the axial load applied. It can also be observed that the axial strain grows linearly with tension, and reaches 0.41% at the end.

Fig. 11 shows the ellipticity-tension responses with different curvatures. It can be noted that the smaller the curvature is, the slower the ellipticity changes, i.e., the stronger the anti-buckling capability of the tube is. When the tension reaches a critical value, the tube suffers from catastrophic growth of ellipticity, which means the occurrence of buckling failure.

As shown in Fig. 12, four ellipticity-curvature curves in the figure are corresponding to four different axial loads. It can be observed that the larger initial tension is, the larger the growth rate of ellipticity will become.

Fig. 13 shows the ellipticity-tension responses corresponding to different loading paths for load type A. $\kappa \rightarrow T$ path means that the tube is first bent to a certain curvature κ = 0.2 with zero tension,

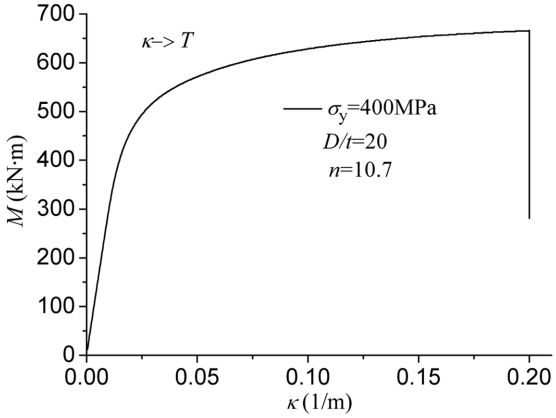

(a) Moment-curvature

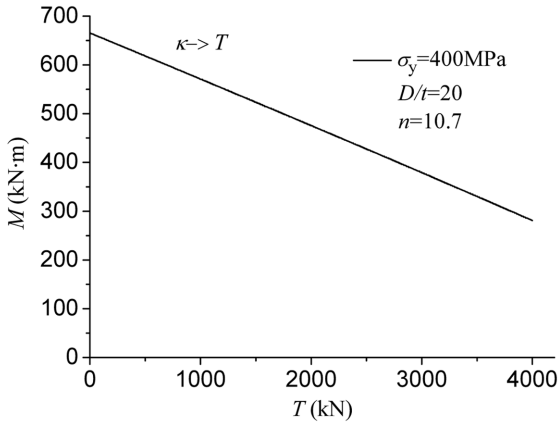

(b) Moment-tension

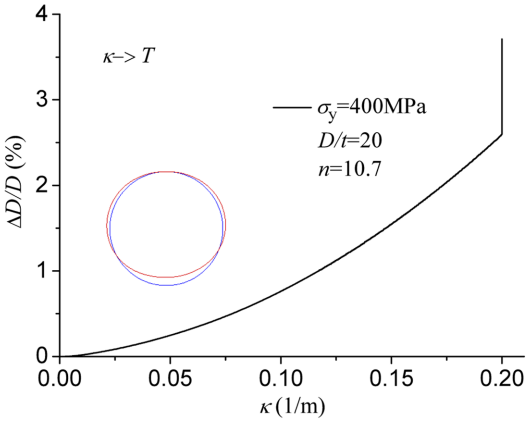

(c) Ellipticity-curvature

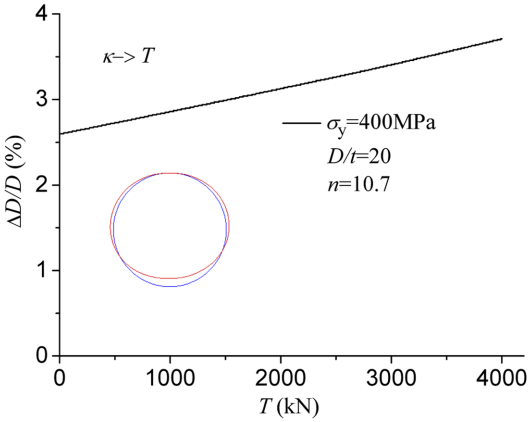

(d) Ellipticity-tension

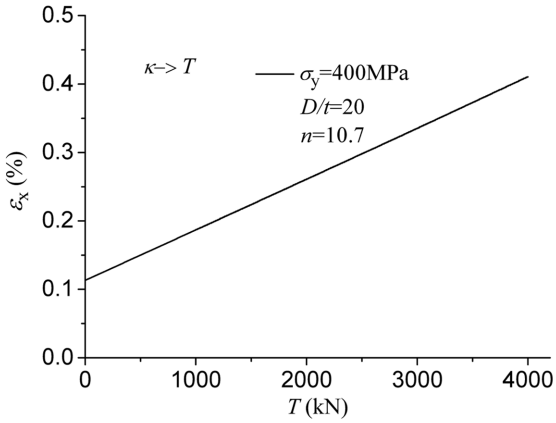

(e) Axial strain-tension

Fig. 10 Predicted responses for $\kappa \rightarrow T$ loading path (Type A)

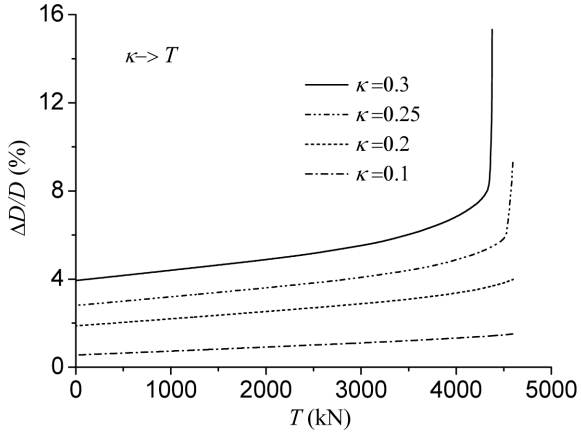

Fig. 11 Ellipticity-tension curves for different curvature

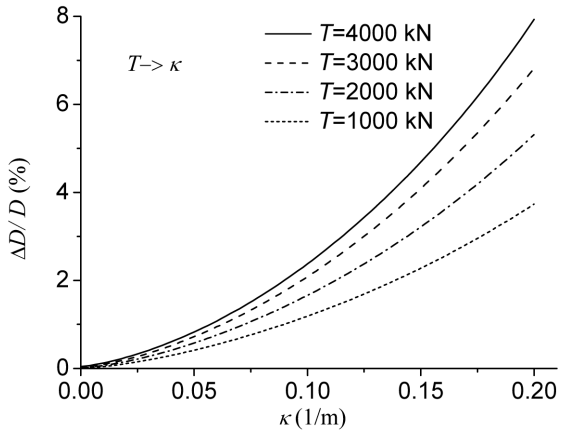

Fig. 12 Ellipticity-curvature curves for different tension

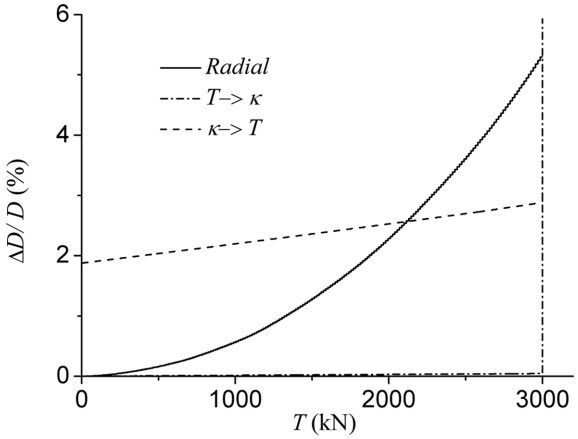

Fig. 13 Ellipticity-tension curves for different loading path (Type A)

and then the tension is increased until T = 3 000 kN is reached with curvature kept constant. Likewise, $T \rightarrow \kappa$ path is to impose tension to the tube first and then bend it into a certain curvature value. As to *Radial* (κ, T) path, the curvature and tension applied on the tube are increased proportionately until κ = 0.2 and T = 3 000 kN. As can be seen from Fig. 13, $T \rightarrow \kappa$ loading path yields the largest ellipticity, and the one corresponding to $\kappa \rightarrow T$ loading path is the smallest. This is due to the fact that the presence of tension accelerates the development of plastic stress and deformation, which is very unfavorable to anti-buckling capacity of the tube.

Included in Fig. 14 are the predicted buckling responses of the tube with its diameter D = 254 mm and D/t = 20 for load type B. As can be seen in the figures, the growth of predicted bending moment is quite close to the one of load type A, i.e., it experiences linear increase, nonlinear increase and subsequent plastic plateau in the bending phase and a linear drop in the tension phase. However, the increase of ellipticity induced in this case is almost unchanged in the tension phase. As to the axial strain, it grows approximately linearly with tension.

Fig. 15 shows how the growth of ellipticity varies when subjected to different initial tension. As

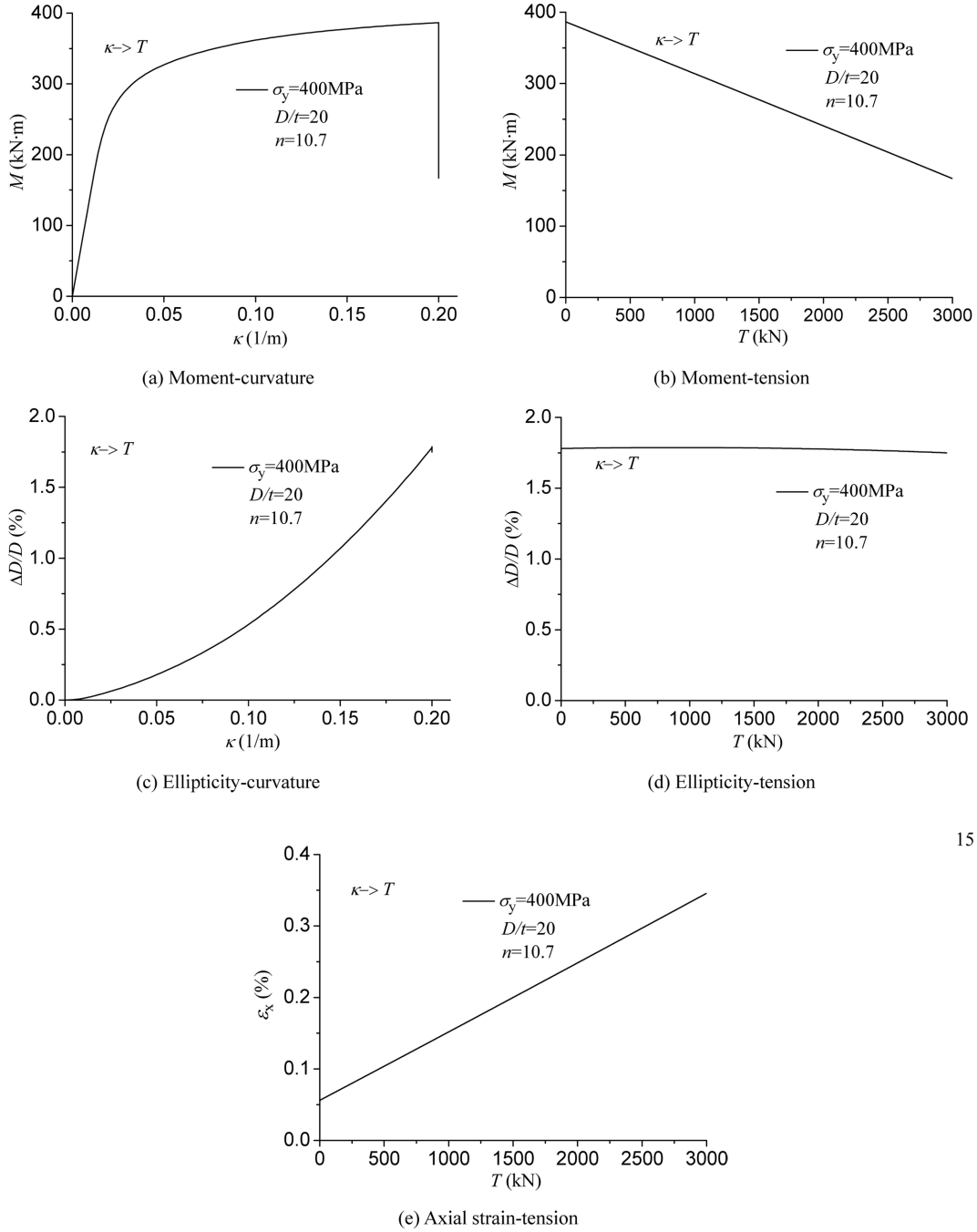

(a) Moment-curvature

(b) Moment-tension

(c) Ellipticity-curvature

(d) Ellipticity-tension

(e) Axial strain-tension

Fig. 14 Predicted responses for $\kappa \rightarrow T$ loading path (Type B)

expected, the larger initial tension is, the larger the rate of growth will be.

Fig. 16 shows the ellipticity-tension responses corresponding to different loading path for load type B with other parameters kept constant. Clearly, the *Radial* (κ, T) path yields the largest

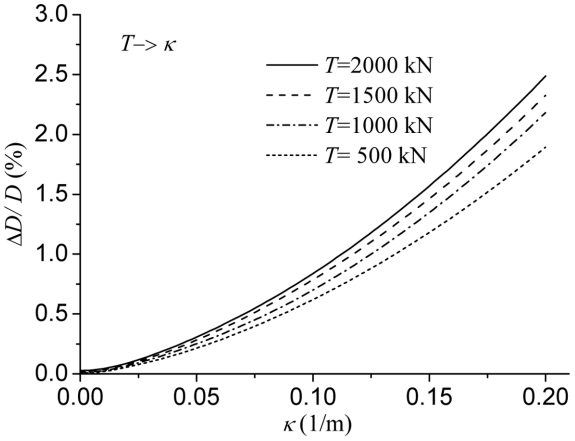

Fig. 15 Ellipticity-curvature curves for different tension

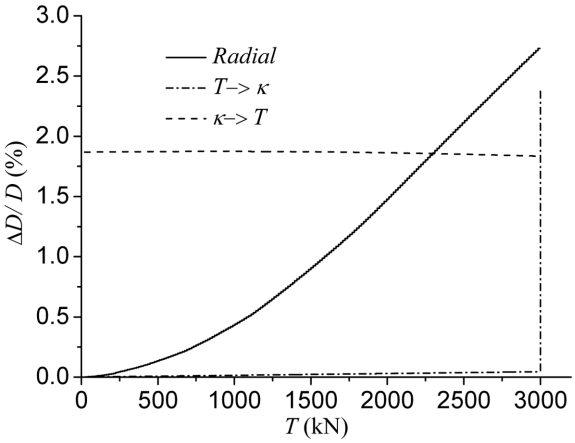

Fig. 16 Ellipticity-tension curves for different loading path

buckling deformation in this case, which reaches 2.73%, about 48.9% higher than that of $\kappa \rightarrow T$ loading path. In addition, it is also worth observing that the predicted ellipticity of $\kappa \rightarrow T$ loading path is less pronounced compared with the other two cases. In other words, the tension would not significantly affect anti-buckling capacity of the tube for $\kappa \rightarrow T$ loading path.

4.3 Parametric study

In this section, the theoretical model is adopted to examine the effects of several important factors including strain-hardening parameter n, yield stress σ_y, as well as diameter-to-thickness ratio (D/t) on buckling behavior of the tubes. The loading path $T \rightarrow \kappa$ for load type A is considered in present section. In addition, the comparison of two load types is carried out. Besides, some discussions and comparisons are made concerning the design of the pipes in practical engineering.

In general, the buckling of the tube is related to some factors, such as the diameter D, wall thickness t, mechanical properties of the material, initial ellipticity, and load history. In addition, residual stress induced in the manufacturing process as well as material yield anisotropy play an important role in the occurrence of the tube buckling. For offshore applications, D/t value ranging from 15 to 70 is recommended. While for deepwater application, D/t value ranging from 15 to 35 is more suitable. In addition, the yield strength of steel for typical offshore pipelines is commonly between 276 MPa and 448 MPa. Besides, the tubes, with initial ellipticity exceeding 0.5%, should be avoided in deepwater applications (Ju and Kyriakides 1991).

Fig. 17 shows that the load type has a significant effect on buckling deformation of the pipe. Following the *Radial* (κ, T) loading path, the tension and curvature applied is prescribed to 4 600 kN and 0.2 for two load types respectively. The results indicate that the transverse force by rigid surface impair the anti-buckling capacity greatly. For load type A, the final ellipticity reaches 8.51%, while for load type B, the pipe only develops an ellipticity of 2.12%. Therefore, in the pipe-laying process the tension applied on the pipe which is bent over the stinger should be minimized to the extent possible.

Fig. 18 shows how the limit moment varies with the material yield stress σ_y with other parameters

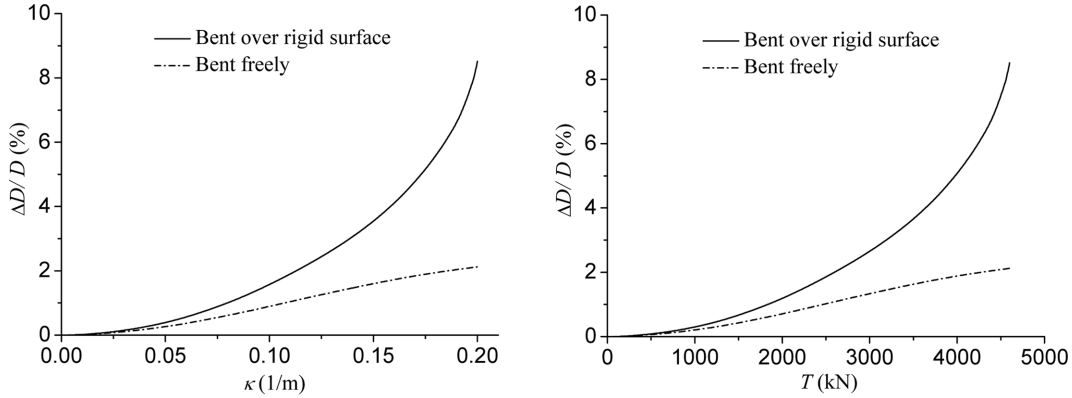

(a) Ellipticity-curvature (b) Ellipticity-tension

Fig. 17 Comparison between buckling responses of two load types

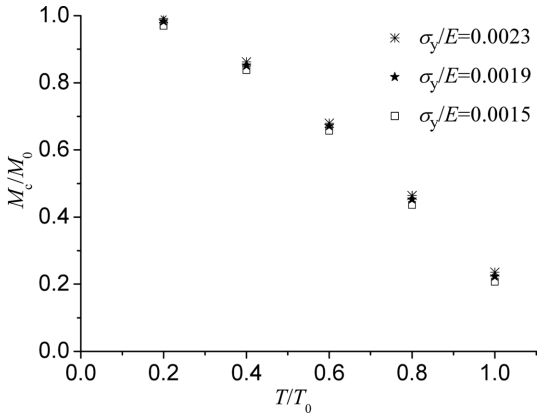

Fig. 18 Effects of yield stress on predicted limit moment and tension

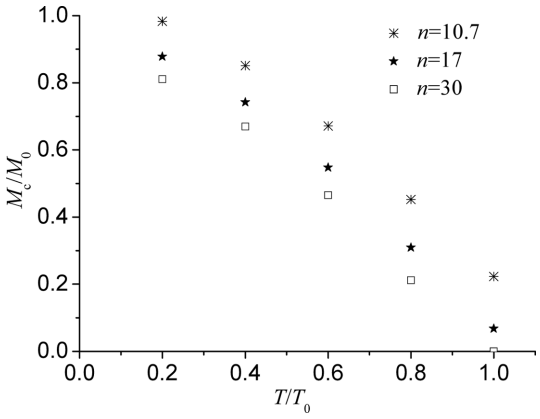

Fig. 19 Effects of strain-hardening parameter on predicted limit moment and tension

kept constant when the axial tension of 0.2, 0.4, 0.6, 0.8 and 1.0 T_0 is first applied to the pipe, respectively. Once attaining the limit moment, localized deformation for a pipe over a stinger in S-lay process would quickly develop in a region of about 5 to 6 tube diameters, which can be taken as the critical state of the buckling. It can be observed from the figure that the tubes with larger yield stress possess little higher limit moment, but the differences are negligible for the same load combination. It is also important to note that the results shown in the figures are normalized to dimensionless factors by the following variables

$$M_0 = D_0^2 t\sigma_0, \qquad T_0 = \pi D_0 t\sigma_0 \tag{20}$$

where mean diameter $D_0 = D - t$, and σ_0 is API yield stress (API 2004), i.e., the stress at a strain of 0.005.

Lower strain-hardening parameter n means larger strain hardening effect. Fig. 19 shows the variation of limit moment and tension with different strain-hardening parameter n. It can be observed that the tubes with lower n can sustain larger limit moment, i.e., higher anti-buckling capacity.

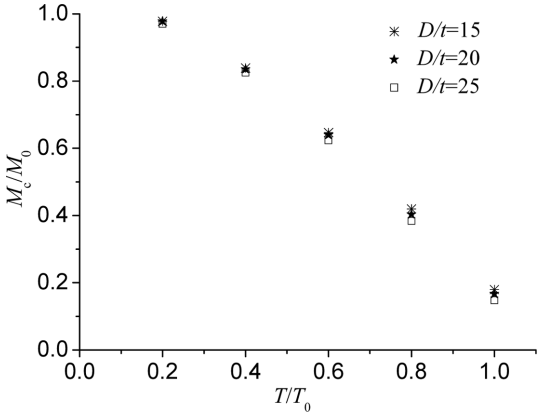

Fig. 20 Effects of *D/t* on predicted limit moment and tension

The effects of diameter-to-thickness ratio (*D/t*) on the limit moment and tension are examined in Fig. 20. Three *D/t* values ranging from 15, 20 and 25 are adopted, while keeping other parameters constant. Just as expected, the limit values corresponding to lower *D/t* tubes are somewhat higher than those of larger *D/t* ones. In addition, it is noted that the degree of its influence varies with different combinations of loads applied.

5. Conclusions

In association with practical pipe-laying circumstances, two different types of loadings, i.e., bent over a rigid surface in the presence of tension, and bent freely in the presence of tension, are taken into account in present study. The buckling behavior of the pipes under various loading paths is presented for both load type A and B. The comparisons of the results obtained respectively by theoretical method and numerical simulation demonstrate that this theoretical model can accurately predict the buckling response of the tubes under combined tension and bending.

In view of the fact that the loading path $T\rightarrow\kappa$ (load type A) could more approximate the load history as the pipes go over a stinger in S-lay operation, a series of parametric studies are conducted adopting the theoretical formulation developed, and the following conclusions can be drawn:

Loading path has a significant effect on the load-carrying capacity and buckling deformation of the tubes. For load type A, $T\rightarrow\kappa$ loading path yields the most severe buckling deformation, while for load type B, the ellipticity of *Radial* (κ, T) loading path is the largest. The tube develops much more severe ellipticity when bent over rigid surface. It is therefore recommended that tension applied on the pipe should be minimized to the extent possible. As to the $T\rightarrow\kappa$ loading path for load type A, different values of load combination will result in great differences of load-carrying capacity and buckling deformation of the tubes.

The strain-hardening parameter n has a significant effect on the buckling behavior of the tube, which will possess stronger resistance to buckling deformation with lower strain-hardening parameter. Whereas, the yield stress σ_y and diameter-to-thickness ratio (*D/t*) seem to be negligible for the case of combined tension and bending.

In summary, it can be concluded that the theoretical model and solution method described in this

context are successfully used to predict the buckling response of offshore pipelines under combined tension and bending in the over-bend segment for deepwater S-lay operation. However, the further research works should be conducted to explore the asymmetric buckling behavior of offshore pipelines under more complicated load conditions.

Acknowledgements

The work of this paper is jointly sponsored by the National Natural Science Foundation of China (Grant No. 51009122), the Fundamental Research Funds for the Central Universities (Grant No. 2010QNA4030), and the National Science and Technology Major Project of China (Grant No. 2011ZX05027-002-005-011). The financial support is greatly appreciated by the authors.

References

Al-Sharif, A.M. and Preston, R. (1996), "Simulation of thick-walled submarine pipeline collapse under bending and hydrostatic pressure", *Proceedings of Offshore Technology Conferences*, Houston, Texas, OTC 8212, USA.

API (American Petroleum Institute) (2004), API Specifications 5L: Specifications for Line Pipe, 43rd Editions, API Publishing Services, Washington DC, USA.

Dyau, J.Y. and Kyriakides, S. (1992), "On the response of elastic-plastic tubes under combined bending and tension", *J. Offshore Mech. Arctic Eng.*, **114**(1), 50-62.

Gellin, S. (1980), "The plastic buckle of long cylindrical shells under pure bending", *Int. J. Solids Struct.*, **16**(5), 397-407.

Gong, S.F., Yuan, L. and Jin, W.L. (2011), "Buckling response of offshore pipelines under combined tension, bending, and external pressure", *J. Zhejiang Univ.-Sci. A*, **12**(8), 627-636.

Kashani, M. and Young, R. (2005), "Installation load consideration in ultra-deepwater pipeline sizing", *J. Transp. Eng.-ASCE*, **131**(8), 632-639.

Hibbitt, H.D., Karlsson, B.I. and Sorensen, P. (2006), *ABAQUS Theory Manual*, Version 6.3, Pawtucket, Rhode Island, USA.

Ju, G.T. and Kyriakides, S. (1991), "Bifurcation buckling versus limit load instabilities of elastic-plastic tubes under bending and external pressure", *J. Offshore Mech. Arctic Eng.*, **113**(1), 43-52.

Kyriakides, S. and Shaw, P.K. (1982), "Response and stability of elastoplastic circular pipes under combined bending and external pressure", *Int. J. Solids Struct.*, **18**(11), 957-973.

Kyriakides, S. and Corona, E. (2007), *Mechanics of Offshore Pipelines*, Volume 1: Buckling and Collapse, Elsevier Science, Oxford, UK, Burlington, Massachusetts.

Li, Z.G., Wang, C., He, N. and Zhao, D.Y. (2008), "An overview of deepwater pipeline laying technology", *China Ocean Eng.*, **22**(3), 521-532.

Sanders, J.L. (1963), "Nonlinear theories of thin shells", *Quart. Appl. Math.*, **21**(1), 21-63.

Shaw, P.K. and Kyriakides, S. (1985), "Inelastic analysis of thin-walled tubes under cyclic bending", *Int. J. Solids Struct.*, **21**(11), 1073-1110.

Simo, J.C. and Armero, F. (1992), "Geometrically non-linear enhanced strain mixed methods and the method of incompatible modes", *Int. J. Numer. Meth. Eng.*, **33**(7), 1413-1449.

Xue, J.H. and Fatt, M.S.H. (2002), Buckling of a non-uniform, long cylindrical shell subjected to external hydrostatic pressure", *Eng. Struct.*, **24**(8), 1027-1034.

Yuan, L., Gong, S.F. and Jin, W.L. (2009), "Analysis on buckling performance of submarine pipelines during deepwater pipe-laying operation", *China Ocean Eng.*, **23**(2), 303-316.